Available online at www.sciencedirect.com
SCIENCE DIRECT®
Intermetallics 11 (2003) 187–195
Intermetallics
www.elsevier.com/locate/intermet

The microstructural evolution of infrared brazed Fe_3Al by BNi-2 braze alloy

Y.L. Lee[a], R.K. Shiue[b], S.K. Wu[a,*]

[a]Department of Materials Science and Engineering, National Taiwan University, Taipei 106, Taiwan
[b]Department of Materials Science and Engineering, National Dong Hwa University, Hualien 974, Taiwan

Received 7 March 2002; accepted 23 May 2002

Abstract

The present work reports a novel approach in joining Fe_3Al by infrared vacuum brazing using BNi-2 (7.0 Cr, 3.1 B, 4.5 Si, 3.0 Fe, 0.06C, and Ni balance) as the brazing filler alloy. Based on the related alloy phase diagrams and solidification theory, the species and morphology of phases in the brazed joint are extensively examined. Many transient phases, including: $(Ni,Fe)_3Al$, $(Ni,Fe)_3(Si,Al)$, $(Fe,Ni,Cr)_3B$ and BCr, were observed after infrared brazing. With increasing the homogenization time of the brazement at 1000 °C, the stoichiometry of both $(Ni,Fe)_3Al$ and $(Ni,Fe)_3(Si,Al)$ phase has changed into $(Ni,Fe)_2Al$ and $(Ni,Fe)_2(Si,Al)$, respectively. Meanwhile, the amounts of the chromium boride and $(Fe,Ni,Cr)_3B$ phases are greatly decreased. Finally, a single-phase joint can be obtained if sufficient time is applied in homogenization treatment of the brazement.

Keywords: A: Iron aluminide; based on Fe_3Al; B: Phase identification; D: Microstructure

1. Introduction

Iron aluminides including Fe_3Al and FeAl have been extensively studied because of their low cost, low density, fairly good corrosion and oxidation resistance [1–3]. Considerable efforts have been focused on both materials processing issues and alloy design of the iron aluminides with modified mechanical and metallurgical properties for structural applications [1,4–20]. The development of a joining process is very important in the application of iron aluminides, but the study of welding and/or brazing iron aluminides is very limited in literatures [2,21–23]. Joining of iron aluminides plays an important role in practical application of such alloys. Welding of iron aluminides is difficult due to its inherent low temperature ductility and poor weldability [23]. Cold cracks can be initiated from the weld even for low energy input processes such as laser welding. Water vapor presence in the atmosphere has shown severe embrittlement of most iron–aluminide alloys during welding [23]. On the other hand, vacuum brazing processed under a high vacuum condition up to 5×10^{-6} mbar provides an alternative bonding technology to join iron aluminides.

Infrared vacuum brazing makes use of infrared energy generated by heating a tungsten filament in a quartz tube as the heating source [24]. The infrared rays can transmit quartz tube and be focused on the specimen. The specimen is locally heated by infrared rays, and the rest of the furnace is not heated during brazing process. Therefore, infrared brazing is a highly potential process with the characteristics of rapid thermal cycle. It has been successfully applied in brazing of TiAl, NiAl and Ni_3Al intermetallics [25–27].

Nickel base braze alloys both have good corrosion resistance and creep strength, so it was selected as filler metal. However, some nickel base braze alloys containing phosphorus are not suitable due to the formation of brittle nickel phosphides. BNi-2 has high creep strength and low liquidus temperature among all Ni base braze alloys. Therefore, it was chosen as a brazing filler metal.

The present work reports a new approach in joining Fe_3Al by infrared brazing using the BNi-2 as brazing filler alloy. The microstructural evolution of the as-brazed joint and the subsequently homogenized brazement will be extensively studied. With the aid of fast infrared heating rate, the early-stage of reaction kinetics in brazed Fe_3Al is also discussed.

* Corresponding author. Tel.: +886-2-2363-7846; fax: +886-2-2363-4562.
E-mail address: skw@ccms.ntu.edu.tw (S.K. Wu).

0966-9795/03/$ - see front matter © 2003 Elsevier Science Ltd. All rights reserved.
doi:10.1016/S0966-9795(02)00252-2

2. Experimental procedures

The Fe_3Al with the nominal composition Fe-28Al (in at.%) was prepared by vacuum arc remelting of high purity (>99.99 wt.%) Fe and Al pellets. The final weight loss of the master alloy was below 0.1 wt.%. A nickel base filler alloy, Nicrobraz® LM alloy tape made by Wall Colmonoy Co., was used as brazing filler alloy, and its chemical composition in weight percent was 7.0 Cr, 3.1 B, 4.5 Si, 3.0 Fe, 0.06C, and Ni balance. Based on the AWS specification of Ni base braze alloys, the chemical composition of Nicrobraz® LM braze is consistent with BNi-2 braze alloy [28]. The solidus and liquidus temperatures of this alloy are 970 and 1000 °C, respectively. The thickness of Nicrobraz® LM tape was 100 μm throughout the experiment.

Compared with traditional furnace brazing, infrared brazing is featured with rapid thermal cycle. Unlike furnace brazing, higher infrared brazing temperature will have less damage to the base metal. Additionally,

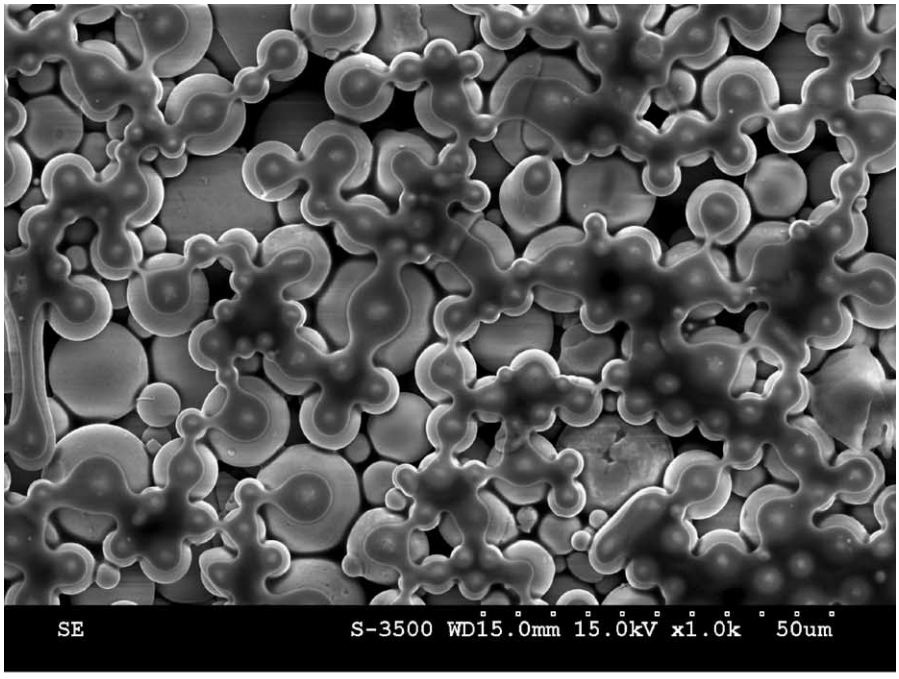

(a)

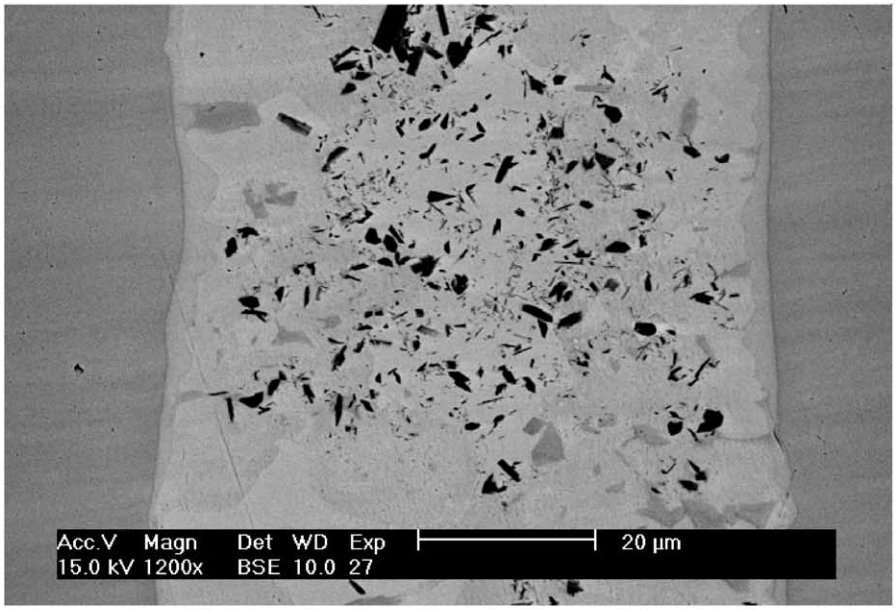

(b)

Fig. 1. SEM observations of (a) Nicrobraz® LM alloy tape prior to infrared brazing, (b) Fe_3Al/BNi-2/Fe_3Al specimens brazed at 1150 °C for 2 s.

high brazing temperature can greatly speed up the microstructural evolution of the brazed joint. Therefore, a temperature 150 °C higher than the liquidus of braze alloy was chosen as brazing temperature. Infrared brazing was performed in a vacuum of 5×10^{-5} mbar at 1150 °C for 2, 24 and 240 s in the study. In order to study the phase stability in the brazed joint, some infrared brazed specimens were subsequently annealed in a vacuum furnace at 1000 °C for 24, 48, 72 and 144 h, respectively. All joined surfaces were firstly polished by SiC papers up to grit 600, and subsequently ultrasonically cleaned by acetone prior to infrared brazing. The area of the LM foil was approximately the same as that of base metal. To enhance the absorption of infrared rays, a graphite fixture was used during brazing. Specimens were sandwiched between two graphite plates. A thermal couple was inserted into the upper graphite plate, and contacted with the brazed specimen. The thickness of Fe_3Al substrate is 1 mm, and the total thickness of Fe_3Al/BNi-2/Fe_3Al joint is about 2 mm. Because the thickness of brazed joint is not very thick, it is reasonable to assume that the temperature gradient in the specimen is negligible. An ULVAC SINKO-RIKO RHL-P610C infrared furnace with the heating rate of 900 °C/min was used throughout the experiment. There is a time delay between the actual specimen temperature and programmer temperature, so time compensation is necessary in the experiment. The brazing time specified in the test is the actual specimen holding time in the experiment [24].

The brazed sample was cut by a low speed diamond saw, and followed by a standard metallographic procedure. The cross section of the brazed specimens was examined using a Philips® XL30 scanning electron microscope (SEM) with an accelerating voltage of 15 kV. Quantitative chemical analysis was performed by using a JEOL JXA-8800M electron probe microanalyzer (EPMA) equipped with a wavelength dispersive spectrometer (WDS). Its spot size is 1 μm, and its operation voltage is 15 kV.

3. Results and discussion

Fig. 1(a) displays the secondary electron image (SEI) of the Nicrobraz® LM alloy tape prior to brazing. It shows the morphology of brazing powders. Fig. 1(b) shows the backscattered electron image (BEI) of SEM observations for Fe_3Al/BNi-2/Fe_3Al specimen brazing at 1150 °C for 2 s. The SEI displays topographic contrast of the cross section in the joint. The BEI does not provide topographic contrast but primarily shows the element distribution in the brazed joint [29]. The morphology of braze alloy after infrared brazing is very different from that of the original powder. It demonstrates the melting of braze alloy powders during infrared brazing. According to Fig. 1(b), the element distribution in the joint is not quite uniform, and many phases can be observed in the joint. Fig. 2 shows the BEI of the infrared brazed specimen at 1150 °C for 24 s. It is noted that huge difference is found in comparison between Figs. 1(b) and 2. According to chemical analysis results, at least two major phases can be identified in Fig. 2, one is the matrix and the other is the gray streak-like boride phase.

Fig. 3 shows the SEM BEI observation and EPMA chemical analysis results of the Fe_3Al/BNi-2/Fe_3Al specimen brazed at 1150 °C for 240 s. Very limited

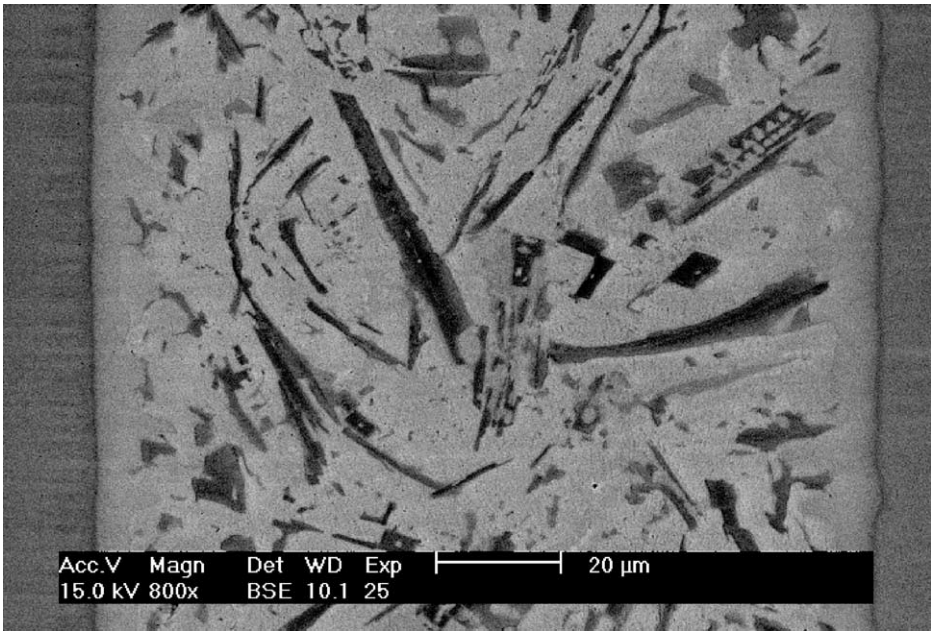

Fig. 2. The BEI of the infrared brazed specimen at 1150 °C for 24 s.

oxygen content is detected in the EPMA analysis, so it implies that there is little oxidation during infrared brazing. Avoiding oxidation during brazing is a prerequisite to obtaining a good bonding. At least five phases can be observed in the analysis. First, the base metal as marked by 1 in Fig. 3 is primarily Fe_3Al substrate solid solution with minor Ni due to the high brazing temperature. A continuous layer close to the interface of Fe_3Al/BNi-2 is shown in Fig. 3 as marked by 2 in the SEM BEI photograph. The phase is mainly comprised of Al, Fe and Ni. Based on the stoichiometric ratio of Ni, Fe and Al in this phase, a $(Ni,Fe)_3Al$ phase is suggested in the analysis. Both Ni_3Al and Fe_3Al phases can be found in related binary alloy phase diagrams, and Fe can be completely dissolved into Ni at elevated temperature [30]. Therefore, it is reasonable to deduce the formation of $(Ni,Fe)_3Al$ phase after infrared brazing. There are three different phases in the central part of the joint. The small black spots marked by 5 in the figure are identified as chromium boride, BCr. It is alloyed with other minor elements, e.g. Fe, Ni, Si and C. Similarly, the gray matrix in the middle part of the joint marked by 3 in the figure can be identified as $(Fe,Ni)_3(Si,Al)$ according to the stoichiometric ratio of Fe, Ni, Si

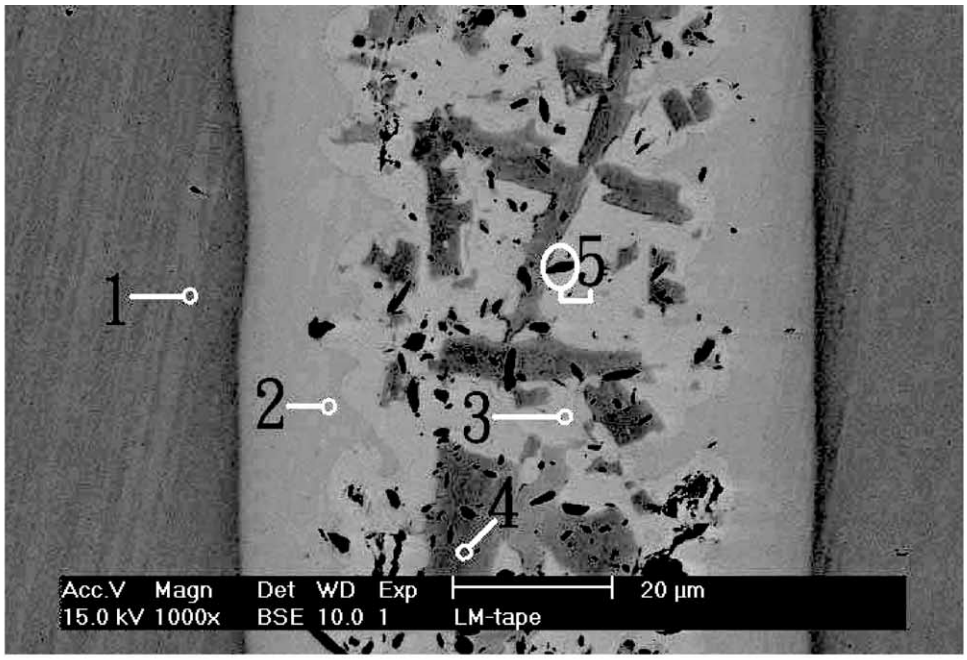

Element	1	2	3	4	5
Al	25.3	23.5	11.9	---	0.2
B	---	0.1	1.6	19.3	45.8
C	---	1.9	2.1	2.1	0.7
Cr	0.1	0.6	0.5	10.1	48.4
Fe	72.0	15.2	6.5	47.0	2.4
Ni	2.6	56.4	64.4	21.4	2.4
O	---	0.2	1.0	---	---
Si	---	2.1	12.0	---	0.1

* all chemical analysis results are shown in at%

Fig. 3. The SEM BEI observation and EPMA chemical analysis results of Fe_3Al/BNi-2/Fe_3Al specimens brazed at 1150 °C for 240 s.

and Al. Finally, the dark gray streak-like phase marked by 4 in Fig. 3 contains B, Cr, Fe and Ni. It is basically a type of boride, and its stoichiometric ratio is close to $(Fe,Ni,Cr)_3B$ phase.

To unveil the transient evolution of the brazed microstructure, a multi-component equilibrium phase diagram is preferred in the study. However, there is no such phase diagram currently available. Therefore, it is essential to consult related ternary alloy phase diagrams [31]. The chemical composition of the LM braze in atomic percent is 6.6 Cr, 14.1 B, 7.9 Si, 2.6 Fe and Ni balance, and the base metal consists of Fe and Al. Fig. 4 displays the liquidus projection of B–Cr–Ni ternary alloy phase diagram in atomic percent [31]. Many important invariant reactions are included in this figure. It is well known that silicon acts as a melting point depressant in BNi-2 braze alloy. According to EPMA chemical analysis as shown in Fig. 3, BCr exists in the braze alloy after infrared brazing. The melting point of BCr is 2100 °C, and the eutectic reaction of a molten braze can explain its formation. On the other hand, select B–Ni–Si ternary phase diagram cannot explain the formation of BCr after infrared brazing. Consequently, the use of B–Cr–Ni ternary alloy phase diagram is important in elucidating the solidification of the braze alloy. Although Si is not included in the B–Cr–Ni

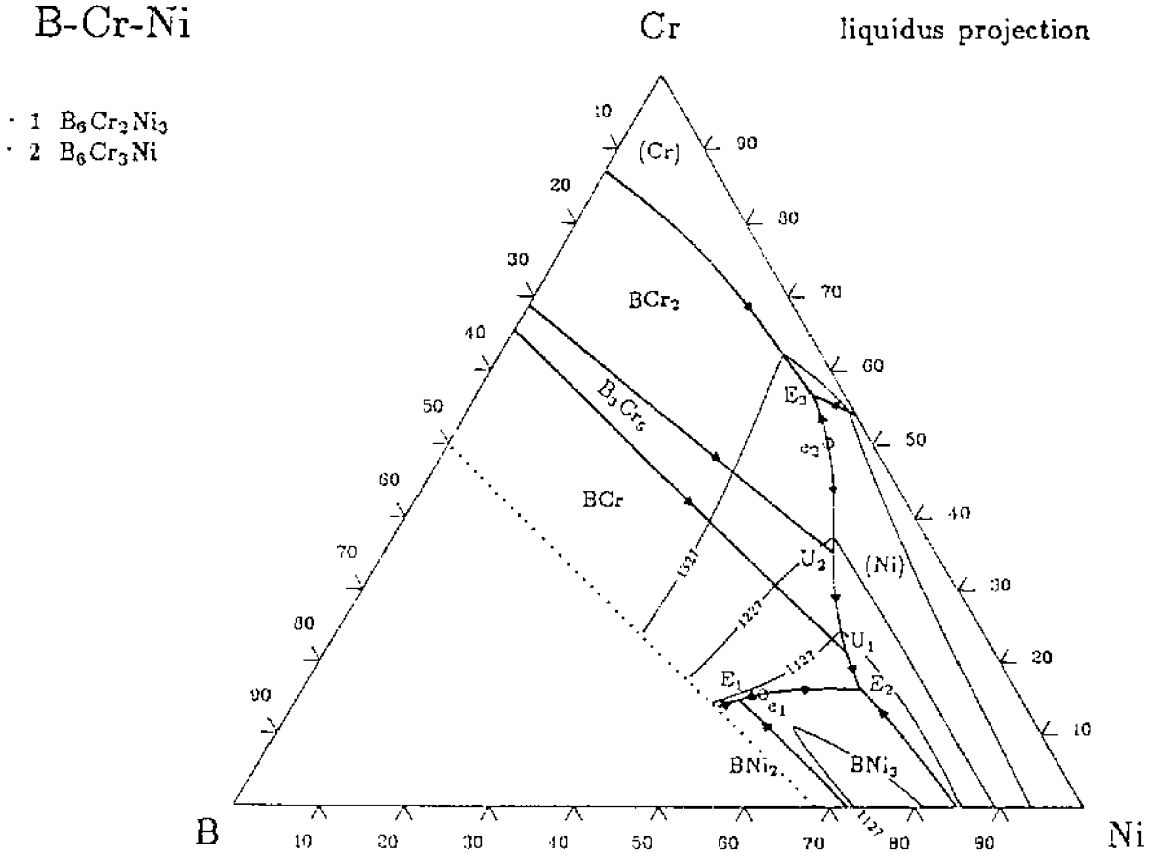

Reaction Scheme

B-Cr-Ni

e_1 :	$l \rightleftharpoons BCr + BNi_3$		
e_2 :	$l \rightleftharpoons BCr_2 + (Ni)$		
E_1 :	$L \rightleftharpoons BCr + BNi_2 + BNi_3$	1096°C	L = 35.6 at.% B , 14.7 at.% Cr
E_2 :	$L \rightleftharpoons BCr + BNi_3 + (Ni)$	1050°C	L = 18.3 at.% B , 16.1 at.% Cr
E_3 :	$L \rightleftharpoons BCr_2 + (Cr) + (Ni)$	1258°C	L = 4.3 at.% B , 57.9 at.% Cr
U_1 :	$L + B_3Cr_5 \rightleftharpoons BCr + (Ni)$	1096°C	L = 17.3 at.% B , 21.2 at.% Cr
U_2 :	$L + BCr_2 \rightleftharpoons B_3Cr_5 + (Ni)$	1220°C	L = 12.3 at.% B , 35.3 at.% Cr

Fig. 4. Liquidus projection of B–Cr–Ni phase diagram [31].

ternary alloy phase diagram, the B–Cr–Ni phase diagram can still provide a first approximation of the phase evolution during infrared brazing.

According to Fig. 4, there are three ternary eutectic reactions, E_1, E_2 and E_3, in the diagram. The chemical composition of the molten BNi-2 braze is located in the primary field of BNi_3 and closes to that of eutectic liquid at E_2 in Fig. 4. The ternary eutectic temperature at E_2 in B–Cr–Ni phase diagram is 1050 °C, which is lower than the brazing temperature (1150 °C) in the experiment. Three phases are expected to form after the eutectic reaction, including BCr, BNi_3 and Ni phase. According to the EPMA chemical analysis shown in Fig. 3, BCr is readily observed after brazing. It is also noted that Fe in the base metal can be dissolved into the molten braze. Consequently, BNi_3 is alloyed with Fe. A new phase $(Fe,Cr,Ni)_3B$ is formed after infrared brazing. The dissolution of Fe and Al elements from Fe_3Al substrate into the molten braze may result in isothermal solidification of the BNi-2 braze alloy during brazing. The Ni phase may react with Fe and Al dissoluted from Fe_3Al matrix. Therefore, no pure Ni phase is observed

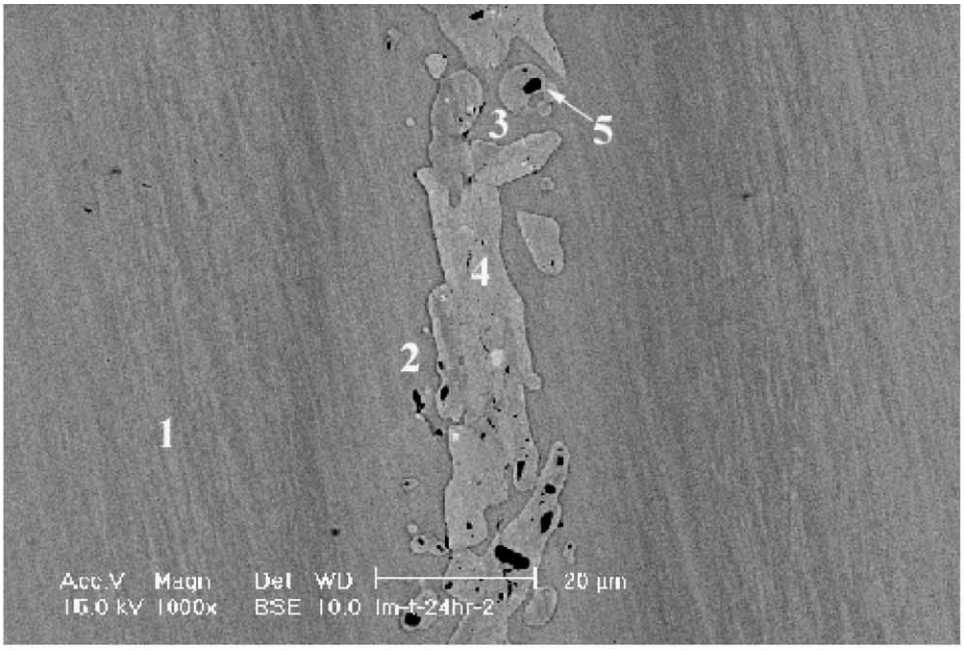

Element	1	2	3	4	5
Al	24.6	31.1	22.5	---	0.1
B	---	0.5	0.1	20.9	41.3
C	1.1	2.2	2.2	2.4	2.1
Cr	---	0.2	0.9	16.6	54.0
Fe	72.9	13.7	18.1	46.6	1.9
Ni	0.7	48.7	48.7	13.5	0.6
O	0.7	0.5	0.6	---	---
Si	---	3.1	6.9	---	---

* all chemical analysis results are shown in at%

Fig. 5. The SEM BEI observation and EPMA chemical analysis results of Fe_3Al/BNi-2/Fe_3Al specimens brazed at 1150 °C for 240 s and followed by 1000 °C for 24 h.

in the joint. The formation of both $(Ni,Fe)_3Al$ close to the interface and $(Ni,Fe)_3(Si,Al)$ in the middle of joint has been observed in this study. According to current experimental results, the kinetics of the solidification path is consistent with the related alloy phase diagrams.

In order to verify the phase stability in the brazed joint, some infrared brazed specimens were subsequently homogenized in a vacuum furnace at 1000 °C for 24, 48, 72 and 144 h, respectively. Fig. 5 shows SEM BEI observation and EPMA chemical analysis results of $Fe_3Al/BNi\text{-}2/Fe_3Al$ specimens brazed at 1150 °C for 240 s and followed by annealing at 1000 °C for 24 h. Compared with Fig. 3, the width of brazed joint is greatly decreased due to high temperature homogenization of the joint. The chemical composition of base metal is close to Fe_3Al as marked by 1 in Fig. 5. The initial as-brazed $(Ni,Fe)_3Al$ phase has changed its stoichiometry into $(Ni,Fe)_2Al$ phase as marked by 2 in Fig. 5. Similarly, the initially as-brazed $(Ni,Fe)_3(Al,Si)$ phase changes its chemical composition close to $(Ni,Fe)_2(Al,Si)$ as marked by 3 in Fig. 5. Two borides, BCr marked by 5 and $(Fe,Cr,Ni)_3B$ marked by 4, are still observed in the figure. It is reasonable that the amount of BCr in the joint is greatly decreased due to the homogenization of the specimen. Meanwhile, both the morphology and the amount of $(Fe,Cr,Ni)_3B$ phase are also changed. The width of the joint is greatly decreased. With increasing homogenization time of the infrared brazed specimen, the width of the joint is consistently decreased as shown in Fig. 6(a)–(c). If the brazed specimen is homogenized at 1000 °C for 120 h, most phases near interface are disappeared. Most of BCr and $(Fe,Cr,Ni)_3B$ phases are dissolved into the Fe_3Al matrix. Consequently, a single-phase joint can be formed if sufficient time is applied in the homogenization treatment.

The interdiffusion between the braze alloy and base material resulting in isothermal solidification may play a crucial role in determining the final microstructure of the joint. The melting point depressants, e.g. boron and silicon, in BNi-2 braze alloy can fast diffuse into Fe_3Al substrate, and Fe_3Al will also dissolute into the molten braze. Both metallurgical phenomena can increase the melting point of the molten braze. Therefore, it is reported that isothermal solidification takes place during traditional furnace brazing using Ni–B–Si filler metal as a result of boron removal from the filler metal [32–34]. A simple $x = (Dt)^{\frac{1}{2}}$ estimation can indicate whe-

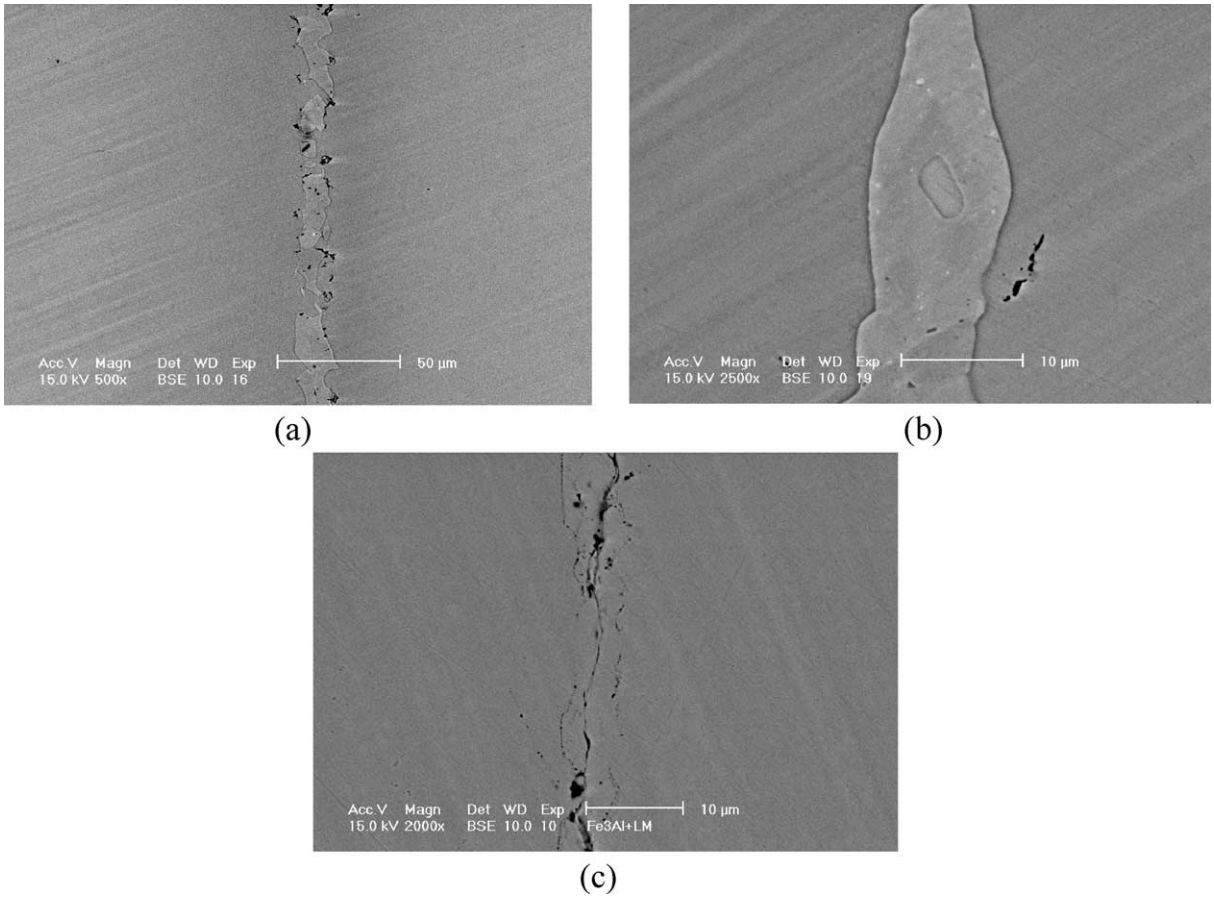

Fig. 6. The SEM BEI observations of $Fe_3Al/BNi\text{-}2/Fe_3Al$ specimens brazed at 1150 °C for 240 s and subsequently followed by 1000 °C homogenization for (a) 48, (b) 72 and (c) 120 h.

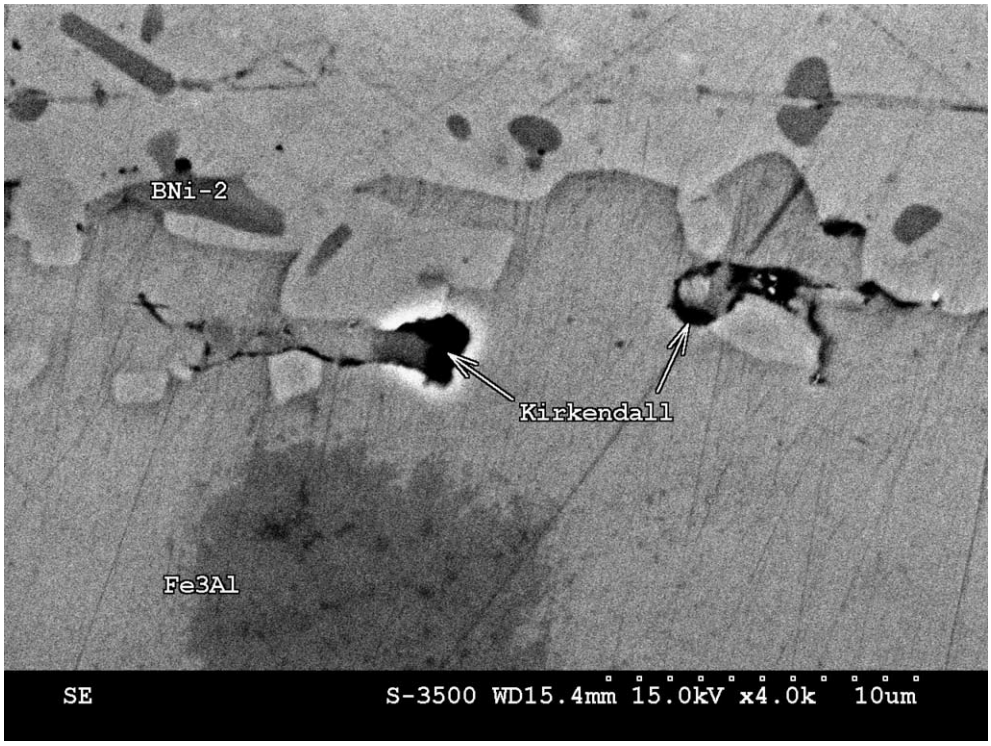

Fig. 7. The SEM SEI observations of Fe_3Al/BNi-2/Fe_3Al specimens brazed at 1150 °C for 240 s and followed by 1000 °C for 24 h.

ther isothermal solidification is possible for these experimental conditions. The diffusion distance (x) is equal to the square root of diffusion coefficient (D) times the time period of diffusion (t). The diffusion coefficient of boron in Fe_3Al at 1150 °C is approximately 4.1×10^{-11} cm^2/s [35]. The estimated diffusion distance of B into Fe_3Al at 1150 °C for 240 s is only about 1 μm. Consequently, the isothermal solidification due to the removal of B from braze alloy is very limited in infrared brazing due to its fast thermal cycle. However, the dissolution rate of Fe_3Al into the molten braze at elevated temperatures needs further study in order to estimate the possibility of isothermal solidification during infrared brazing.

The subsequent homogenization treatment of brazement results in interdiffusion of elements between substrate and the solidified braze alloy. However, the diffusivity of B is much higher than that of other elements. It will cause nonsymmetrical mass transport during interdiffusion. As demonstrated in Fig. 7, some Kirkendall porosity (about 1–2 microns) close to the braze is observed. The Kirkendall effect describes that the vacancy will be formed if the rate of interdiffusion is not balanced [36]. Boron is a very small atom, and it can diffuse much faster than Al, Si, Cr, Ni and Fe atoms with a larger atomic radius. Therefore, boron can fast diffuse into substrate driven by concentration gradient, but much slower diffusion rates of Al and Fe atoms into the solidified braze are expected. Consequently, vacancy will be formed after heat treatment.

4. Conclusion

A novel approach in joining Fe_3Al by infrared vacuum brazing using BNi-2 as the brazing filler alloy is performed in the study. The species and morphology of phases in the brazed joint are extensively examined. Many transient phases, including: $(Ni,Fe)_3Al$, $(Ni,Fe)_3(Si,Al)$, $(Fe,Ni,Cr)_3B$ and BCr, were observed after infrared brazing. With increasing the homogenization time of the brazement at 1000 °C, the stoichiometry of both $(Ni,Fe)_3Al$ and $(Ni,Fe)_3(Si,Al)$ phase has changed into $(Ni,Fe)_2Al$ and $(Ni,Fe)_2(Si,Al)$. Most of BCr and $(Fe,Cr,Ni)_3B$ phases can be dissolved into the Fe_3Al matrix during homogenization of the brazement, so the amounts of the chromium boride and $(Fe,Ni,Cr)_3B$ phases are decreased with the time increment of homogenization. Finally, a single-phase joint can be obtained if sufficient time is applied in homogenization treatment of the brazement.

Unlike traditional furnace brazing, the interdiffusion between the braze alloy and base metal is very limited during infrared brazing due to its rapid thermal cycle. The subsequent homogenization treatment of brazement results in interdiffusion of elements between the substrate and the solidified braze alloy. Since the diffusivity of B is much higher than that of other elements, it will cause nonsymmetrical mass transport during interdiffusion. Therefore, fine Kirkendall porosity (about 1–2 microns) close to the braze is observed in the experiment.

Acknowledgements

The authors gratefully acknowledge the financial support from National Science Council (NSC), Republic of China, under the grants NSC 89-2216-E002-002. EPMA analysis by Ms. Shu-Yueh Tsai in NSC Instrument Center, National Tsing Hua University, Hsinchu, Taiwan, is also gratefully acknowledged.

References

[1] Liu CT, George EP, Maziasz PJ, Schneibel JH. Mat Sci Eng A-Struct A258 1998:84.
[2] Stoloff NS. Mat Sci Eng A-Struct A258 1998:1.
[3] Stoloff NS, Sikka VK. Physical metallurgy and processing of intermetallic compounds. New York, NY: Chapman and Hall; 1996.
[4] Davies RG, Stoloff NS. Acta Metall 1963;11:1187.
[5] Liu CT. High-temperature order intermetallic alloys. In: Baker I, Darolia R, Whittenberger JD, Yoo MH, editors. V. MRS Symp. Proc. 288. Pittsburgh, USA: MRS; 1993. p. 3.
[6] Agarwal A, Dahotre NB. Scripta Mater 2000;42:493.
[7] Deevi SC. Intermetallics 2000;8:679.
[8] Sundar RS, Baligidad RG, Prasad YVRK. Mat Sci Eng A-Struct A258 1998:219.
[9] Blackford JR, Buckley RA, Jones H, Sellars CM. J Mater Sci 1998;33:4417.
[10] Hajaligol MR, Deevi SC, Sikka VK. Mat Sci Eng A-Struct A258 1998:249.
[11] Chakraborty SP, Sharma IG, Bose DK. J Alloy Compd 1998; 280:255.
[12] McKamey CG, Maziasz PJ. Intermetallics 1998;6:303.
[13] Baligidad RG, Prakash U, Rao VR. ISIJ Int 1996;36:1448.
[14] Subramanian R, Schneibel JH. JOM-J Min Met Mat S 1997; 49:50.
[15] Agwarwal A, Akhtar MJ, Balasubramaniam R. J Mater Sci 1996; 31:5207.
[16] Deevi SC, Sikka VK, Liu CT. Prog Mater Sci 1997;42:177.
[17] Mistler RE, Sikka VK, Scorey CR, McKernan JE, Hajaligol MR. Mat Sci Eng A-Struct A258 1998:258.
[18] Blackford JR, Buckley RA, Jones H, Sellars CM. Scripta Mater 1996;34:721.
[19] Balasubramaniam R. J Alloy Compd 253- 1997;4:148.
[20] Balasubramaniam R. Scripta Mater 1996;34:127.
[21] Jung SB, Minamino Y, Yamane T, Saji S. J Mater Sci Lett 1993; 12:1684.
[22] Fasching AA, Edwards GR, David SA. Sci Technol Weld Joi 1997;2:167.
[23] Fasching AA, Ash DI, Edwards GR, David SA. Scripta Metall 1995;32:389.
[24] Shiue RK, Wu SK. O JM, Wang JY Metall Mater Trans A 2000; 31A:2527.
[25] Lee SJ, Wu SK, Lin RY. Acta Mater 1998;46:1283.
[26] Lee SJ, Wu SK, Lin RY. Acta Mater 1998;46:1297.
[27] Yang TY, Wu SK, Shiue RK. Intermetallics 2001;9:341.
[28] Olson DL, Siewert TA, Liu S, Edwards GR. ASM handbook (Vol. 6). Materials Park, OH: ASM International; 1993.
[29] Lee RE. Scanning electron microscopy and X-ray microanalysis. 1993
[30] Massalski TB. Binary alloy phase diagrams. Materials Park, OH: ASM International; 1990.
[31] Villars P, Prince A, Okamoto H. Handbook of ternary alloy phase diagrams. Metals Park, OH: ASM International; 1995.
[32] Kubachewski O, Alcock CB, Spencer PJ. Materials thermochemistry. New York, NY: Pergamon Press; 1993.
[33] Shyam A, Suwas S, Bhargava S. Prakt Metallogr 1997;34:264.
[34] Gale WF, Wallach ER. J Mater Sci 1992;27:5653.
[35] Hasaka M, Morimura T, Kondo S-I. Scripta Metall Mater 1993; 29:967.
[36] Humpston G, Jacobson DM. Principles of soldering and brazing. Metals Park, OH: ASM International; 1993.